Molecular Microbiology (2011) 82(4), 998–1014 ■

doi:10.1111/j.1365-2958.2011.07882.x
First published online 27 October 2011

Corynebacterium glutamicum survives arsenic stress with arsenate reductases coupled to two distinct redox mechanisms

Almudena F. Villadangos,[1†] Karolien Van Belle,[2,3,4†] Khadija Wahni,[2,3,4] Veronica Tamu Dufe,[2,4,6] Sofia Freitas,[2,3,4] Haneen Nur,[2,3,4] Sandra De Galan,[5] José A. Gil,[1] Jean-Francois Collet,[2,6] Luis M. Mateos[1] and Joris Messens[2,3,4*]**

[1]*Department of Molecular Biology, Area of Microbiology, University of León, León, Spain.*
[2]*Brussels Center for Redox Biology, Brussels, Belgium.*
[3]*VIB, Department of Structural Biology, Brussels, Belgium.*
[4]*Structural Biology Brussels and* [5]*Analytical Chemistry, Vrije Universiteit Brussel, Brussels, Belgium.*
[6]*de Duve Institute, Université catholique de Louvain, Brussels, Belgium.*

Summary

Arsenate reductases (ArsCs) evolved independently as a defence mechanism against toxic arsenate. In the genome of *Corynebacterium glutamicum*, there are two arsenic resistance operons (*ars1* and *ars2*) and four potential genes coding for arsenate reductases (Cg_ArsC1, Cg_ArsC2, Cg_ArsC1' and Cg_ArsC4). Using knockout mutants, *in vitro* reconstitution of redox pathways, arsenic measurements and enzyme kinetics, we show that a single organism has two different classes of arsenate reductases. Cg_ArsC1 and Cg_ArsC2 are single-cysteine monomeric enzymes coupled to the mycothiol/mycoredoxin redox pathway using a mycothiol transferase mechanism. In contrast, Cg_ArsC1' is a three-cysteine containing homodimer that uses a reduction mechanism linked to the thioredoxin pathway with a k_{cat}/K_M value which is 10^3 times higher than the one of Cg_ArsC1 or Cg_ArsC2. Cg_ArsC1' is constitutively expressed at low levels using its own promoter site. It reduces arsenate to arsenite that can then induce the expression of Cg_ArsC1 and Cg_ArsC2. We also solved the X-ray structures of Cg_ArsC1' and Cg_ArsC2. Both enzymes have a typical low-molecular-weight protein tyrosine phosphatases-I fold with a conserved oxyanion binding site. Moreover, Cg_ArsC1' is unique in bearing an N-terminal three-helical bundle that interacts with the active site of the other chain in the dimeric interface.

Accepted 3 October, 2011. For correspondence. *E-mail joris.messens@vib-vub.be; Tel. (+32) 2 6291992; Fax (+32) 2 6291963; **E-mail luis.mateos@unileon.es; Tel. (+34) 987291126; Fax (+34) 987291409. †Contributed equally.

Introduction

In bacteria, the principal arsenic detoxification mechanism is based on the reduction of intracellular arsenate to arsenite by cytoplasmic arsenate reductase enzymes (ArsCs). Arsenite is pumped out of the cell by specific arsenite efflux pump systems (Achour *et al.*, 2007). ArsCs are small cytoplasmic redox enzymes intensely studied during the last two decades (Mukhopadhyay and Rosen, 2002; Messens and Silver, 2006). For reduction, ArsC makes use of electrons coming from the cellular redox system. Electrons are transferred from NADPH by the sequential involvement of three different thiolate nucleophiles, but different mechanisms arose independently during evolution (Messens and Silver, 2006). Based on these reduction mechanisms, four distinct ArsC classes can be defined: (i) the thioredoxin (Trx)/thioredoxin reductase (TrxR)-dependent class with the structural fold of low-molecular-weight protein tyrosine phosphatase (LMW-PTPase) (Fig. 1A left) and with the three thiolate nucleophiles on a single ArsC enzyme (plasmid pI258 of *Staphylococcus aureus*) (Zegers *et al.*, 2001) (Sa_ArsC in Fig. 1B), (ii) the glutathione (GSH)/glutaredoxin (Grx)-coupled class with only one thiolate nucleophile on the enzyme such as prokaryotic ArsCs with a glutaredoxin-fold (plasmid R773 of *Escherichia coli*) (Fig. 1A right; Ec_ArsC in Fig. 1C) and eukaryotic (Gladysheva *et al.*, 1994) ArsCs with sequence similarity to the rhodanese/Cdc25 phosphatase superfamily (Acr2p from *Saccharomyces cerevisiae*) (Mukhopadhyay and Rosen, 1998), (iii) the trypanothione/trypanothione reductase class with a rhodanese/Cdc25 phosphatase fold (*Leishmania major*) (Mukhopadhyay *et al.*, 2009), and finally (iv) the mycothiol

(MSH)/mycoredoxin (Mrx)-dependent class in Actinobacteria that we recently described for *Corynebacterium glutamicum* (Ordóñez *et al*., 2009) (Cg_ArsC1 and Cg_ArsC2 in Fig. 1B). Thus, different classes of arsenate reductases use different reducing systems.

One of the major and perhaps the most efficient reducing system in cells is the thioredoxin (Trx) system (Collet and Messens, 2010). As an alternative source of reducing equivalents, cells have millimolar concentrations of LMW thiols. GSH is the most extensively studied LMW thiol (Masip *et al*., 2006), but other Cys-derived LMW thiols such as mycothiol (Rawat and Av-Gay, 2007; Jothivasan and Hamilton, 2008) and the structurally related bacillithiol, likely play roles in thiol/disulphide homeostasis (Fahey, 2001; Helmann, 2011). Arsenate reductases exploit the most efficient reducing systems for the reduction of arsenate. For example, in the Gram-positive *Bacillus subtilis*, the ArsC activity from the chromosomal SKIN element is coupled to Trx (Bennett *et al*., 2001; Guo *et al*., 2005) and not to bacillithiol. In *S. aureus*, pI258 ArsC is also Trx coupled even when CoA-SH is here proposed to be a major LMW thiol (delCardayre *et al*., 1998). The linkage to a specific cellular reduction system doesn't seem to be related to the structural fold of the arsenate reductases. For example, SynArsC from *Synechocystis* sp. (Syn_ArsC in Fig. 1B) with the same LMW-PTPase structural fold as pI258 Sa_ArsC (PDB ID 2 L17) (Yu *et al*., 2011) depends on GSH/Grx (Li *et al*., 2003) and not on the Trx reduction system.

Arsenate reductases depend for the reduction of arsenate to arsenite on a single cell-specific redox system. However, in the genome of *C. glutamicum*, we found the first documented example in which arsenate reductases with a similar structural fold (Fig. 1A) use different reducing system within the same organism. Some use the MSH/Mrx system (Cg_ArsC1/C2), while others depend on Trx for the reduction of arsenate (Cg_ArsC1'). The Trx-coupled Cg_ArsC1' reduces arsenate to arsenite during the first contact of the bacterium with arsenate. The produced arsenite can then induce the expression of Cg_ArsC1 and Cg_ArsC2.

Results

Cg_ArsC1' is constitutively expressed, Cg_ArsC1 and Cg_ArsC2 only after exposure to arsenite

To search for a function of *Cg_arsC1'* and *Cg_arsC4*, we analysed on immunoblots the expression of all the arsenate reductases in *C. glutamicum* before and after exposure to arsenite, which has been shown to inactivate the ArsR repressor (Ordóñez *et al*., 2008). We purified Cg_ArsC2, Cg_ArsC1' and Cg_ArsC4 from *E. coli* BL21(DE3) containing the corresponding pET derivative vectors (see Table S1), and immunized rabbits. The antibodies were IgG-enriched and specificity was tested. The anti-Cg_ArsC2 antibodies recognize Cg_ArsC2, Cg_ArsC1 and Cg_ArsC1' (Fig. S1A). Not surprisingly, because Cg_ArsC1 is similar in sequence to Cg_ArsC2. That anti-Cg_ArsC2 also faintly recognizes Cg_ArsC1' is not a problem for this analysis, because both enzymes show a distinct migration on SDS-PAGE (Fig. S1A). The same is true for the cross-reactivity of anti-Cg_ArsC1' antibodies (Fig. S1B). The anti-Cg_ArsC4 antibodies are specific (Fig. S1C).

In *C. glutamicum*, Cg_ArsC2 and Cg_ArsC1 were only expressed after exposure to arsenite (Table 1). No bands for Cg_ArsC1' or Cg_ArsC4 were detected.

To rule out possible detection limitations, we added the codons for a His_8-tail to the 3′ end of the chromosomal copy of *Cg_arsC1*' and *Cg_arsC4* by using a suicide plasmid recombination system. After a 20-fold protein concentration of cellular extracts from strain ArsC1'His on Ni^{2+}-IMAC, we observed expression of Cg_ArsC1' under induced and non-induced conditions (Table 1; Fig. S1B, lanes 3–4). In similar conditions no band for Cg_ArsC4 was detected (Table 1; Fig. S1C, lanes 3–4). To conclude, Cg_ArsC2 and Cg_ArsC1 are only expressed after exposure of *C. glutamicum* to arsenic stress, while Cg_ArsC1' seems to be constitutively expressed, although at a low level.

Cg_ArsC1′ is constitutively transcribed

As the expression of Cg_ArsC1' is low, we also decided to quantify the transcriptional level of *Cg_arsC1*' in different strains and under different conditions. Quantitative reverse transcriptase PCR analyses (Table 2) were performed with mRNA isolated from *C. glutamicum* wild type (RES167), and from the mutant strains 2Δars [in which the two chromosomal *ars* operons are removed (Fig. 2A)] and ArsC1 (in which the *Cg_arsC1* gene has been disrupted) (Ordóñez *et al*., 2009), and this in the absence or presence of 1 mM arsenite.

We took the high Cycle Threshold (*CT*) values of the 2Δars strain (no *ars1* operon present for primer amplification) as a background reference (high *CT* values) and 16S rDNA as positive control (low *CT* value) (Table 2). In the wild-type strain, mRNA of *Cg_acr3-1* [the arsenite permease gene of the same *ars1* operon (Fig. 2A)] was only found (lower *CT* value compared with 2Δars) in the presence of arsenite, while we observed mRNA of *Cg_arsC1*' in the absence and the presence of arsenite. The level of mRNA of *Cg_arsC1*' is higher in the presence of arsenite, because it is induced (240 times) by the two upstream promoters [P*arsC1* and P*acr3-1* (Fig. 2A)] (Ordóñez *et al*., 2005). To avoid this induction, we disrupted the *Cg_arsC1* gene located on the *ars1* operon in between *Cg_acr3-1* and *Cg_arsC1*' (Fig. 2A). In this ArsC1 mutant strain,

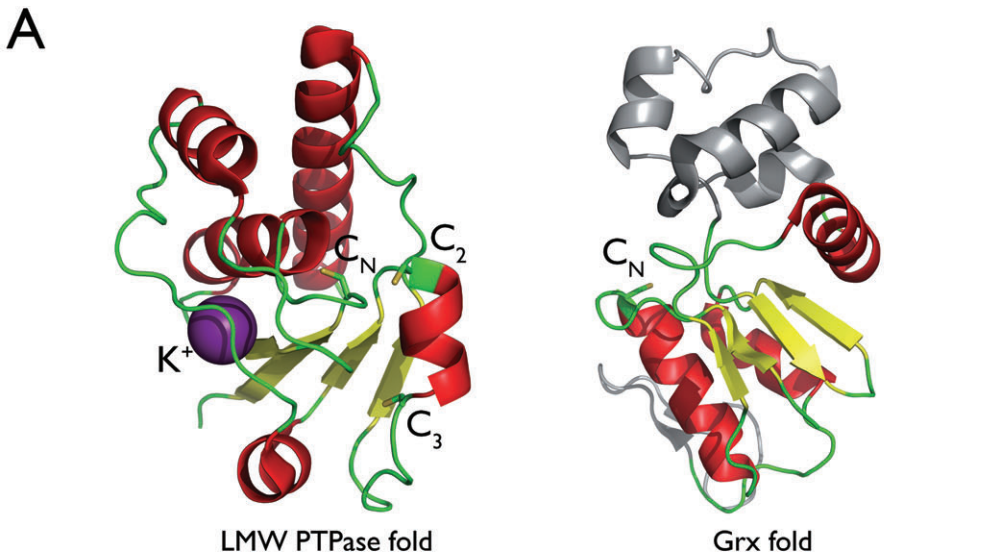

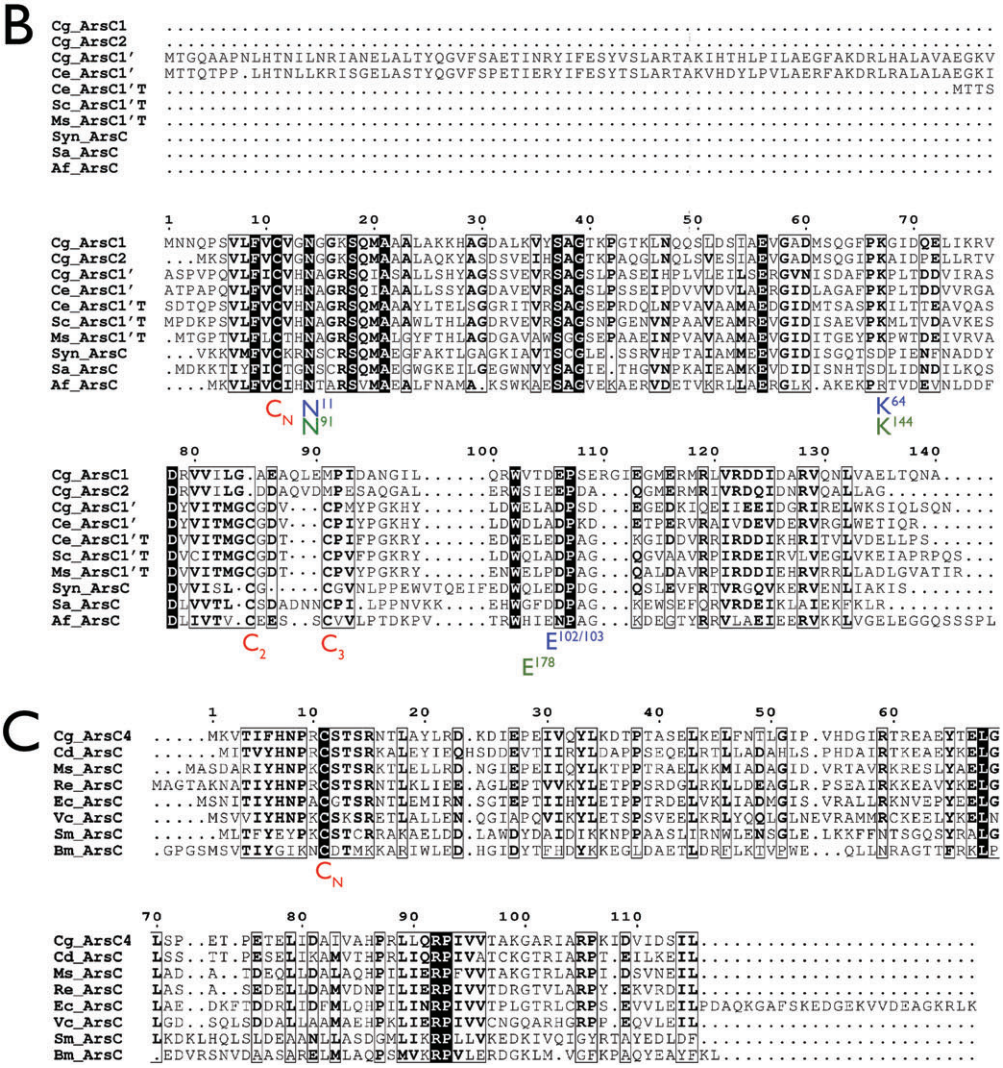

Fig. 1. The ArsC1′ and ArsC4 arsenate reductase subgroups of *C. glutamicum*.
A. Ribbon diagram of the overall structures of pI258 Sa_ArsC (PDB ID 1LJL) with a LMW PTPase-fold (left) as representative for the ArsC1′ subgroup of arsenate reductases (B), and R773 Ec_ArsC (PDB ID 1I9D) with a Grx-fold (right) as representative for the ArsC4 subgroup (C). The essential cysteines in the order of involvement during catalysis are indicated (C_N = nucleophilic cysteine). In pI258 Sa_ArsC, the positive charge of the potassium (K^+) is essential for stability and activity; cysteines C82 and C89 from Sa_ArsC are indicated as C_2 and C_3. The figure was generated using MacPyMol (Delano Scientific LLC 2006).
B. CLUSTALW alignment (Chenna *et al.*, 2003) of the arsenate reductases corresponding to the ArsC1′ and ArsC1'T subgroup: *C. glutamicum* (Cg_ArsC1′, Cg_ArsC1 and Cg_ArsC2), *Corynebacterium efficiens* YS314 [Ce_ArsC1′ (CE0878) and Ce_ArsC1'T (CE0877)], *Streptomyces coelicolor* A3(2) [Sc_ArsC1'T (SC03700)], *Mycobacterium smegmatis* MC2-155 (Ms_ArsC1'T (MSMG_1171)], *Synechocystis* sp. PCC6803 (Syn_ArsC), *Staphylococcus aureus* from pI258 (Sa_ArsC) and *Archaeoglobus fulgidus* DMS 4304 [Af_ArsC (AF1361)]. The truncated Cg_ArsC1'T was obtained by deletion of the 78 aa from protein Cg_ArsC1′ (first line of the Cg_ArsC1′ alignment).
C. CLUSTALW alignment (Chenna *et al.*, 2003) of the arsenate reductases corresponding to the ArsC4 subgroup: *C. glutamicum* (Cg_ArsC4), *Corynebacterium diphtheriae* NCTCC13129 [Cd_ArsC (DIP0965)], *Mycobacterium smegmatis* MC2-155 [Ms_ArsC (MSMG_5428)], *Rhodococcus equi* [Re_ArsC (REQ_11890)], *E. coli* from R773 (Ec_ArsC), *Vibrio cholerae* [Vc_ArsC (VCV511445)], *Streptococcus mutans* strain UA159 [(Sm_ArsC (SMU_1651)] and *Brucella mellitensis* 2KOK (Bm_ArsC). Important residues are indicated under the alignments (blue for Cg_ArsC2, green for Cg_ArsC1′).

arsenite independent mRNA levels were found for *Cg_arsC1*'. Levels are 50–60 times higher than in the background 2Δars strain and similar to the wild-type RES167 strain without induction (Table 2). As such, *Cg_arsC1*' seems to be also under the control of a constitutive promoter (Table 2). These findings inspired us to search for the constitutive promoter for the transcription and translation of *Cg_arsC1*'.

Cg_ArsC1' uses an arsenite independent promoter

With the Neural Network Promoter Prediction program (Kulp *et al.*, 1996), a possible promoter site was found in the intergenic space (75 nucleotides) between *Cg_arsC1* and *Cg_arsC1′* (Fig. 2A). A larger 160 bp fragment containing the predicted promoter was PCR-amplified obtaining P*arsC1*'.

We quantified the strength of the predicted promoter P*arsC1*' in *C. glutamicum* promoter sequence probe vectors (pEGFP and pEMel-1 derivatives; Table S1) in the absence and presence of various arsenite concentrations using the genes for green fluorescent protein (Fig. 2B) and melanin as reporter (Fig. S2). Fluorescence analyses showed arsenite independent expression with P*arsC1*' (strain containing plasmid pEGFParsC1') while the promoters P*acr3-1* (plasmid pGFP-EP) and P*arsC1* (plasmid pGFP-ER) depend on arsenite (Fig. 2B). Similar results were obtained when the reporter gene was melanin (Fig. S2). As such, P*arsC1*' is a functional constitutive promoter for the expression of Cg_ArsC1'.

Table 1. The expression of arsenate reductases in *C. glutamicum*.

C. glutamicum	Cg_ArsC1/2	Cg_ArsC1′		Cg_ArsC4	
	crude	crude	Conc[a]	crude	Conc[a]
Non-induced	–	–	+	–	–
Induced[b]	+	–	+	–	–

a. Ni^{2+}-IMAC concentrated.
b. Overnight induction with 1 mM As(III) or 5 mM As(V).
The results of immunoblots (Fig. S1) with anti-Cg_ArsC2 (Fig. S1A), anti-Cg_ArsC1′ (Fig. S1B) and anti-Cg_ArsC4 (Fig. S1C) antibodies are summarized.

Table 2. Constitutive transcription of *Cg_arsC1′*.

	Cg_acr3-1			*Cg_arsC1′*			*16S rRNA*	
Strains	–As(III)	+As(III)	I*	–As(III)	+As(III)	I*	–As(III)	+As(III)
RES167	32.16 ± 1.13	25.17 ± 0.88	127 ×	28.10 ± 0.03	20.19 ± 0.86	240 ×	19.35 ± 0.46	18.95 ± 0.66
2Δars	33.39 ± 1.03	33.88 ± 1.22	No	32.79 ± 1.27	33.49 ± 071	No	20.35 ± 0.60	19.70 ± 0.60
ArsC1	31.53 ± 0.92	25.39 ± 0.09	70 ×	27.09 ± 0.85	27.58 ± 0.94	No	18.52 ± 0.46	18.45 ± 0.46

I* = fold induction based on the ratio of 2^{CT} before and after the addition of As(III).
The *CT* values after qRT-PCR analyses of the genes *Cg_acr3-1* and *Cg_arsC1′* from the *C. glutamicum ars1* operon are shown. The *CT* values obtained for the *16S rRNA* genes were used as control for constitutive and highly transcribed genes.

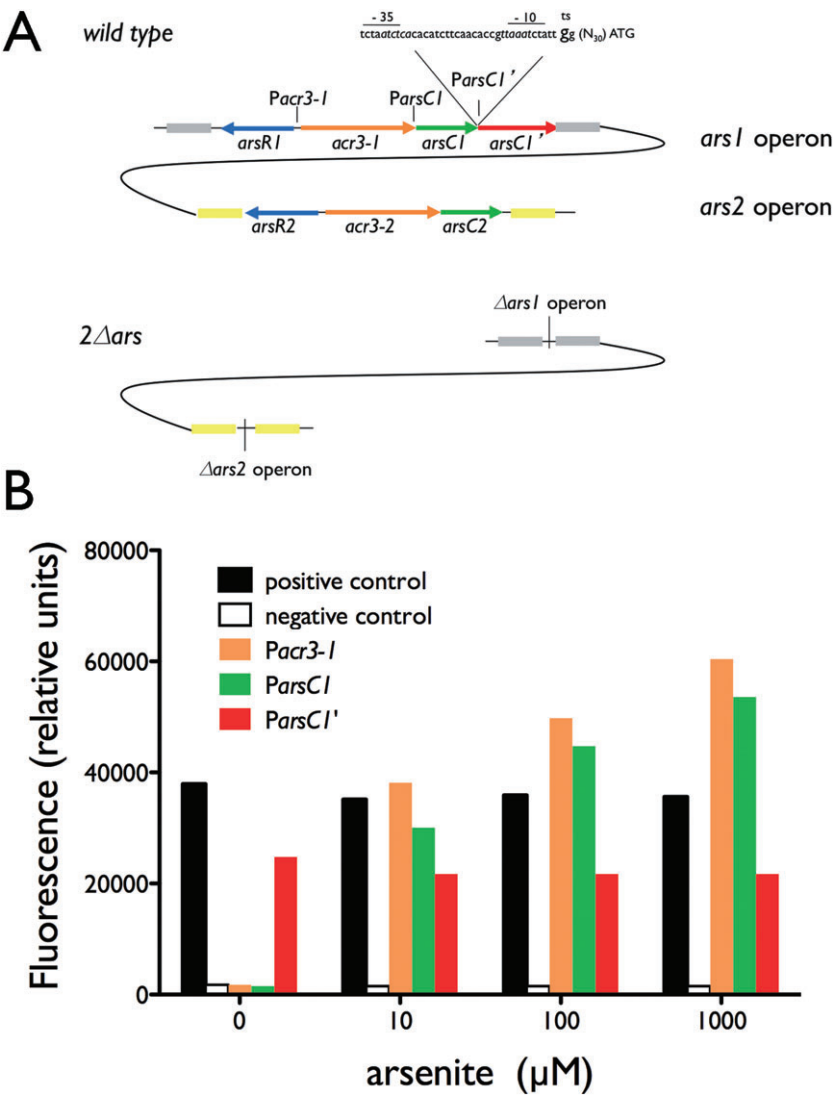

Fig. 2. *Cg_arsC1'* is constitutively transcribed from P*arsC1'*.
A. Structures of the *ars1* and *ars2* operons in wild-type and 2Δars strains of *C. glutamicum*. P*acr3-1* and P*arsC1* are the arsenite-inducible promoters, P*arsC1'* is the constitutive promoter. The sequence for the P*arsC1'* promoter (–10 and –35) and the hypothetical +1 nucleotide is indicated (ts). *arsR1* and *arsR2* encode for the arsenite inducible repressors, *acr3-1* and *acr3-2* for the arsenite permeases, *arsC1*, *arsC2* and *arsC1'* for the arsenate reductases.
B. Promoter strength of P*acr3-1*, P*arsC1* and P*arsC1'* using the bifunctional vector containing the gene for green fluorescent protein (GFP) as reporter. *C. glutamicum* transconjugants containing plasmid pEGFP were used as positive control, whereas those with pEGNC were the negative control (lacking the P*kan* promoter). Strains containing plasmids pGFP-EP (P*acr3-1*) and pGFP-ER (P*arsC1*) show inducible GFP expression (depending on arsenite), whereas strains containing pEGFParsC1' (P*arsC1'*) show constitutive (non-inducible) GFP expression.

Cg_ArsC1' is functional in vivo *under As(V) stress*

Since Cg_ArsC1' is expressed at low levels from its own promoter, we checked whether Cg_ArsC1' has *in vivo* arsenate reductase activity. Surprisingly, the *Cg_arsC1'* knockout strain and the RES167 control strain both survived 60 mM arsenate. Complementation of a double arsenate reductase mutant strain (ArsC1–C2) with *Cg_arsC1'* (pECarsC1') or with the *ars1* chromosomal cluster *Cg_arsC1–Cg_arsC1'* (pECarsC1–C1′) resulted in no additional arsenate resistance due to Cg_ArsC1'.

As no direct arsenate resistance could be attributed to the presence of the *Cg_arsC1'* gene, we measured the steady-state level of arsenic, As(III) and As(V) 60 min after the exposure of *C. glutamicum* mutant strains to 100 μM arsenate using induced coupled plasma mass spectrometry and atomic fluorescence spectroscopy (Table 3). In the RES167 strain, almost no As was accumulated, showing an optimal functioning arsenic defence mechanism. In the 2Δars mutant strain, the steady-state level of arsenite [As(III)] is about the level of the RES167 strain. In 2Δars, all three expressed arsenate reductases Cg_ArsC1, Cg_ArsC2 and Cg_ArsC1' are absent, no

Table 3. Cg_ArsC1' is functional *in vivo*.

Strains	As[a] (ppb)	As(III)[b] (ppb)	As(V)[b] (ppb)
RES167	1.7 ± 0.2	1.4 ± 0.4	0.4 ± 0.2
2Δars	12.2 ± 2.6	1.6 ± 0.2	13.1 ± 3.9
ArsC1–C2	16.4 ± 1.1	5.0 ± 0.3	10.0 ± 0.9
MshC	16.2 ± 1.9	4.8 ± 0.2	8.0 ± 0.6

a. Measured with ICP-MS.
b. Measured with AFS.
Steady-state levels of arsenic, arsenate and arsenite of three independent measurements are shown. *C. glutamicum* strains have been exposed to 100 μM arsenate for 60 min. Data were obtained from 'resting cells'.

Table 4. Kinetic parameters of arsenate reductases linked to different thiol nucleophiles.

ArsCs[a]	Redox mechanism	K_M mM	k_{cat} min^{-1}	k_{cat}/K_M M^{-1} s^{-1}	References
Cg_ArsC1'	Trx	$(32 \pm 4) \times 10^{-3}$	5.6 ± 0.2	2.9×10^3	This work
Cg_ArsC1'T	Trx	110 ± 18	30 ± 2.8	4.5	This work
Cg_ArsC4	Δ nucleophile[b]	NA	NA	NA	This work
Cg_ArsC1	MSH/Mrx1	142	32	3.8	Ordóñez *et al.* (2009)
Cg_ArsC2	MSH/Mrx1	82	17	3.4	Ordóñez *et al.* (2009)
Sa_ArsC pI258	Trx	68×10^{-3}	215	5.2×10^4	Messens *et al.* (2002a)
Ec_ArsC R773	GSH/Grx2	15	32	35	Gladysheva *et al.* (1994)

a. Cg, *C. glutamicum*; Sa, *S. aureus;* Ec, *E. coli.*
b. Trx, MSH/Mrx1 and GSH/Grx2 have been tested as electron donor.
NA, no activity.

As(III) is being produced, and As(V) persists. However, in the ArsC1–C2 or the MshC mutant strain As(III) accumulates. In those strains, the MSH-dependent arsenate reductases are not expressed (ArsC1–C2) or no mycothiol has been produced (MshC). Here, As(V) is still being reduced to As(III), which might be attributed to Cg_ArsC1' that seems to be a functional arsenate reductase *in vivo.*

Cg_ArsC1' produces arsenite coupled to the Trx pathway

Within the Cg_ArsC1' protein sequence identity group (Fig. 1B), two clearly different protein subgroups are observed: (i) those with a high sequence identity along the full length of the Cg_ArsC1' sequence, and (ii) a second subset of arsenate reductase sequences with a high sequence identity with the C-terminal domain of Cg_ArsC1' and where the N-terminal segment of 78 residues is absent (Cg_ArsC1'T). Therefore, we decided to express the whole *Cg_arsC1'* gene and a truncated gene *Cg_arsC1'T* (lacking the 78 N-terminal residues of the corresponding protein) in *E. coli* BL21(DE3). Recombinant proteins were purified to homogeneity on a Ni^{2+}-IMAC column followed by a size exclusion column and molecular weights were confirmed with mass spectrometry (Table S2). Cg_ArsC1' with a molecular weight of 25 360 Da eluted from the size exclusion column as a dimer (~60 kDa), while Cg_ArsC1'T (17 046 Da) was found to be monomeric in solution (~25 kDa) (Fig. S3). On SDS-PAGE, Cg_ArsC1'T showed the tendency to form disulphide linked dimers, while Cg_ArsC1' migrates as a single monomeric band in the absence of DTT (inset of Fig. S3).

In the next step, we reconstituted the redox pathway towards Cg_ArsC1' and Cg_ArsC1'T by following the rate of NADPH consumption. In the presence of mycothiol (MSH), mycoredoxin 1 (Cg_Mrx1) and mycothiol disulphide reductase (Cg_MTR), no NADPH consumption was observed with 100 mM arsenate as substrate (Fig. 3A) and no arsenite was produced (Fig. 4). However in the presence of purified Cg_Trx (*trxA*; NCgl2985) and Cg_TrxR (*trxB*; NCgl2984), Cg_ArsC1' and Cg_ArsC1'T were found to be functional enzymes, linking the reduction of arsenate with the consumption of NADPH (Fig. 3B). As both Cg_ArsC1' and Cg_ArsC1'T use a similar mechanism as described for pI258 *S. aureus* ArsC, and tetrahedral oxyanions like phosphate and sulphate have been shown to stabilize pI258 ArsC during the assay (Messens *et al.*, 2002a), we tested the stability of Cg_ArsC1' and Cg_ArsC1'T in the kinetic assay. Progress curves were plotted against initial enzyme concentration multiplied by time at different enzyme concentrations, and this in the presence and absence of the oxyanion sulphate (Fig. S4) (Selwyn, 1965). We found that Cg_ArsC1' is stabilized in the presence of sulphate (compare Fig. S4A and B), while for Cg_ArsC1'T no sulphate is required to stabilize the protein during the course of the assay (Fig. S4C).

Under the optimized conditions in the reaction coupled to the Trx pathway, Cg_ArsC1' and Cg_ArsC1'T follow Michaelis–Menten kinetics (Fig. 3C and D). The rates of arsenate to arsenite conversions and the K_M values for Cg_ArsC1' were found to be in the same range as for Sa_ArsC pI258 (Table 4). For Cg_ArsC1'T, which lacks the N-terminal domain, the kinetic parameters were greatly reduced and in the same range as found for Cg_ArsC1 or Cg_ArsC2 (Table 4). As such, the N-terminal domain seems not only to be involved in the dimerization of the protein (Fig. S3), but also has an influence on the kinetics of this Trx-dependent arsenate reductase. Although weakly and constitutively expressed, Cg_ArsC1' has a catalytic efficiency (k_{cat}/K_M) which is 10^3 times higher compared with Cg_ArsC1 and Cg_ArsC2 (Table 4).

With atomic fluorescence spectroscopy, we showed that both Cg_ArsC1 and Cg_ArsC1'T produce arsenite in the presence of arsenate (Fig. 4A and B). We checked whether all components of the pathway (Cg_Trx, Cg_TrxR and NADPH) are strictly necessary for electron transfer. Samples with only Cg_Trx and Cg_ArsC1' (Fig. 4A) or

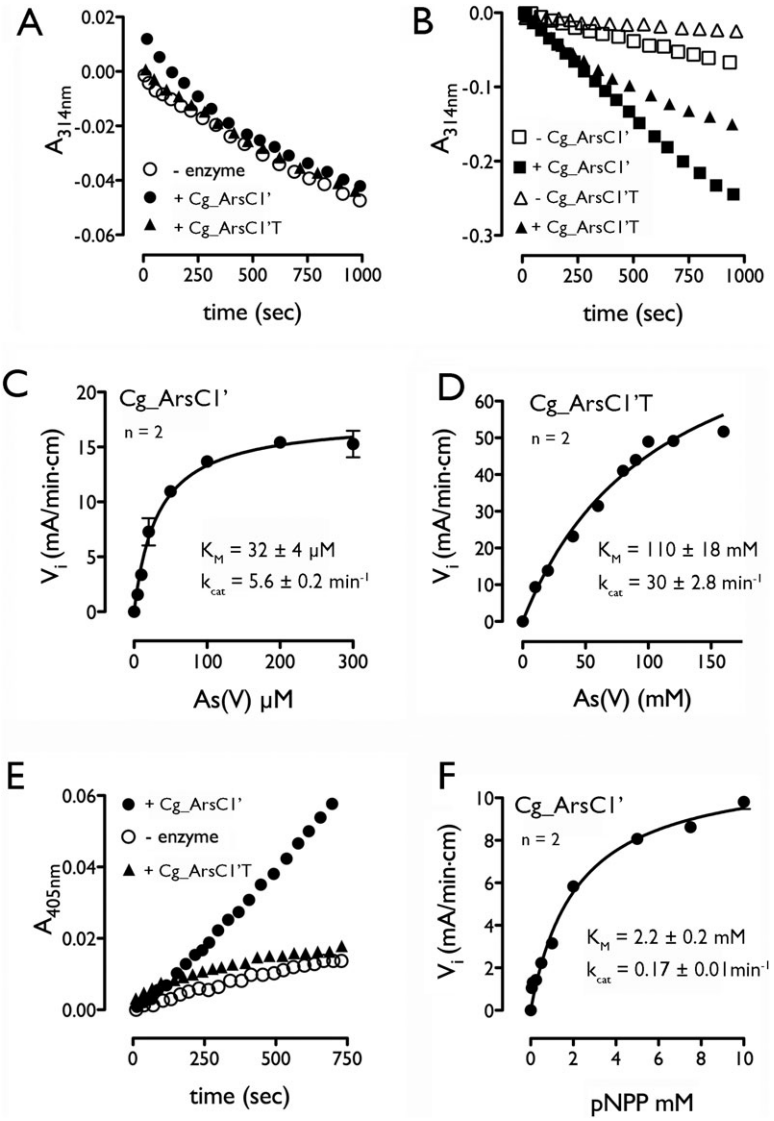

Fig. 3. Cg_ArsC1' is a Trx-coupled arsenate reductase with phosphatase activity.
A. Cg_ArsC1' and Cg_ArsC1'T are not receiving electron from the MSH/Mrx1 pathway. Progress curves of Cg_ArsC1' (200 nM) and Cg_ArsC1'T (200 nM) in 100 mM arsenate with the MSH/Cg_Mrx1/NADPH redox pathway are shown.
B. Cg_ArsC1' and Cg_ArsC1'T are coupled to the Trx pathway. Progress curves of Cg_ArsC1' (500 nM) and Cg_ArsC1'T (500 nM) in the presence 100 mM As(V) with the Cg_Trx/Cg_TrxR/NADPH redox pathway are shown.
C. Michaelis–Menten curve with 500 nM Cg_ArsC1' in the presence of varying As(V) concentrations with 10 µM Cg_Trx, 2 µM Cg_TrxR, 250 µM NADPH in 50 mM Tris/HCl, pH 8.0, 75 mM K_2SO_4 is shown.
D. Same conditions as in (B) but with 500 nM Cg_ArsC1'T in the absence of K_2SO_4 (K_2SO_4 is not stabilizing Cg_ArsC1'T as shown in Fig. S4C).
E. Cg_ArsC1' has phosphatase activity. Progress curves of Cg_ArsC1' (5 µM) and Cg_ArsC1'T (5 µM) in 10 mM pNPP are shown.
F. Michaelis–Menten curve with 3.75 µM Cg_ArsC1' in the presence of varying concentrations of pNPP in 100 mM Na citrate, pH 6.7, 150 mM KCl, 0.1 mM EDTA is shown.
For all the Michaelis–Menten curves the average of two independent experiments are used.

Cg_ArsC1'T (Fig. 4B) produce similar amounts of arsenite as samples containing all the components. The Trx pathway with TrxR and NADPH is only essential to recycle the arsenate reductases via Trx, which clearly indicates a similar arsenate reduction mechanism as described for pI258 Sa_ArsC (Messens *et al.*, 2002b). As Cg_ArsC2 and Cg_ArsC1' are using a distinct redox relay mechanism (Table 4), we decided to solve the structure of both enzymes.

Cg_ArsC2 is the first single cysteine arsenate reductase with a LMW-PTPase structural fold

For Cg_ArsC2, we solved the structure to a resolution of 1.7 Å. Cg_ArsC2 consists of a LMW-PTPase fold, and has a single cysteine in its active-site loop (Fig. 5A). Although Cg_ArsC2 has only a sequence identity of 27% with pI258 Sa_ArsC (PDB code 1LJL) (Messens *et al.*, 2002b), both arsenate reductases are structurally the same (r.m.s.d. of 1.08 Å for 98 of the Cα atoms). Important to note is the absence in Cg_ArsC2 of the functional and flexible redox helix flanked by two cysteine residues as observed in pI258 Sa_ArsC [compare Fig. 1A (left) with Fig. 5A]. The catalytic site is composed of the oxyanion-binding P-loop [including the nucleophilic C8, the conserved N11, and K14 (an Arg in Sa_ArsC and in Cg_ArsC1')] (Fig. 5B). On C8, we observe the formation of a sulphonic acid, which indicates that this cysteine is very sensitive to oxidation, which is also reflected by its low pK_a of ~ 6.2 (Fig. S5). For Cg_ArsC1, which presents an identity of 66% with Cg_ArsC2, a similarly low pK_a value of 6.4 was measured (Fig. S5).

In Cg_ArsC2, there is no potassium binding site. This potassium binding site is an interesting feature observed

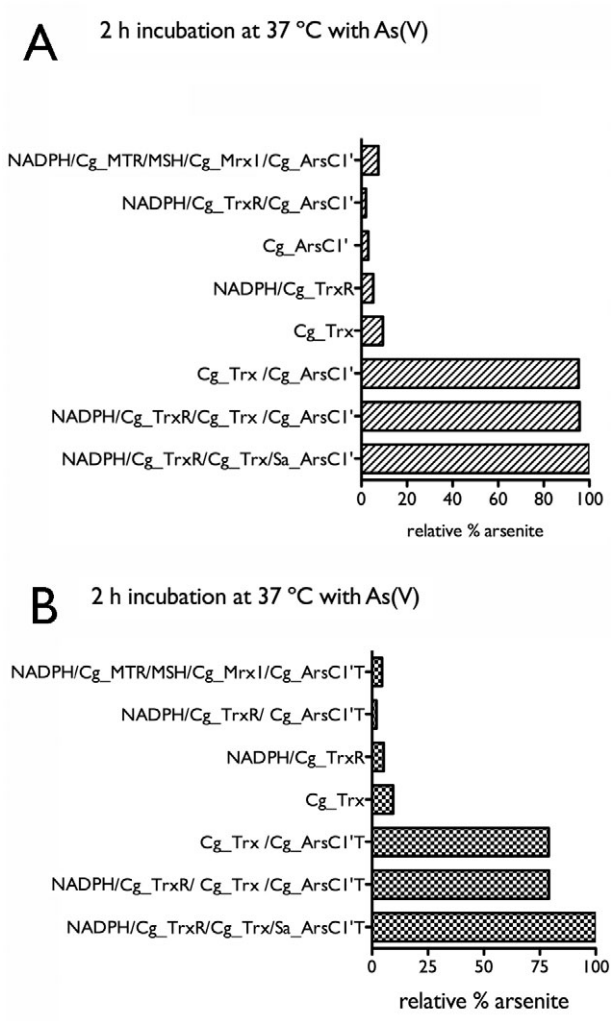

Fig. 4. Cg_ArsC1' and Cg_ArsC1'T catalyse the Cg_Trx-dependent reduction of arsenate to arsenite.
A. Relative percentages of the produced As(III) after 2 h incubation of 500 nM Cg_ArsC1' with varying sample compositions in the presence of 300 μM As(V) are shown. Incubation was performed in 50 Tris/HCl, pH 8.0 as buffer solution using the respective concentrations of the arsenate reductase assay compounds.
B. The same concentrations as in (A) were used, except that 500 nM Cg_ArsC1'T was incubated in the presence of 75 mM As(V). The reaction with Cg_Mrx1, MSH and Cg_MTR was performed as described (Ordóñez *et al.*, 2009).

in pI258 Sa_ArsC (Lah *et al.*, 2003), as K^+ binding stabilizes the structure of Sa_ArsC and increases the specific activity with a factor of 5 (Lah *et al.*, 2003; Roos *et al.*, 2006) [Fig. 1A (left)]. Structurally, potassium is here as part of a hydrogen bonding network that decreases the pK_a of the nucleophilic cysteine thiol in pI258 Sa_ArsC (Roos *et al.*, 2004). In Cg_ArsC2, the charged $N^{\zeta}H^+$ of the conserved Lys^{64} (K64 in Fig. 1B) takes over the role of the potassium as the start of a hydrogen-bonding network via the $O^{\delta 1}$ and the backbone NH of N11 to the S^{γ} of the nucleophilic cysteine C8 (Fig. 5B).

Cg_ArsC1' is a homodimer that combines a LMW-PTPase structural fold with an N-terminal helical bundle

We solved the structure of Cg_ArsC1' in its reduced form to a resolution of 2.2 Å using seleno-methionine single

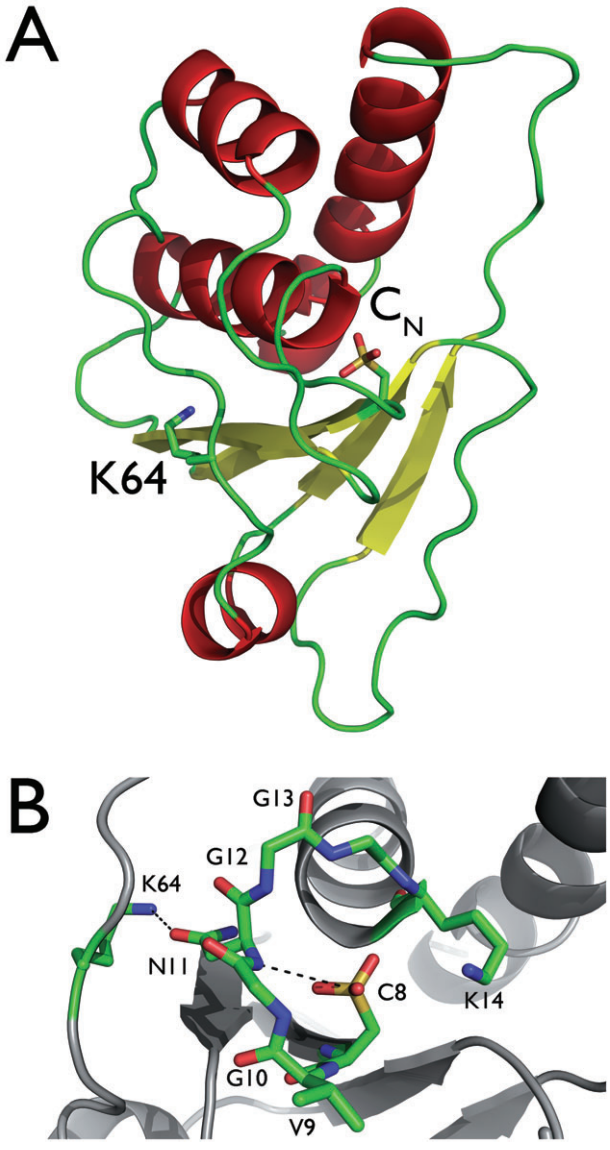

Fig. 5. The structure of Cg_ArsC2 has a LMW-PTPase fold.
A. Ribbon diagram of the overall structure of Cg_ArsC2. The nucleophilic cysteine 8 (C_N) and lysine 64 (K64) are shown.
B. Detailed view on the active-site loop of Cg_ArsC2. The hydrogen-bonding network via the asparagine 11 (N11), which is conserved in the β-conformation (Ramachandran plot gives phi = 52.02° and psi = 34.85°) among arsenate reductases with a LMW-PTPase fold, to the sulphur of cysteine 8 (C8) is indicated. The sulphur of nucleophilic cysteine is oxidized to a sulphonic acid. The figure was generated using MacPyMol (Delano Scientific LLC 2006).

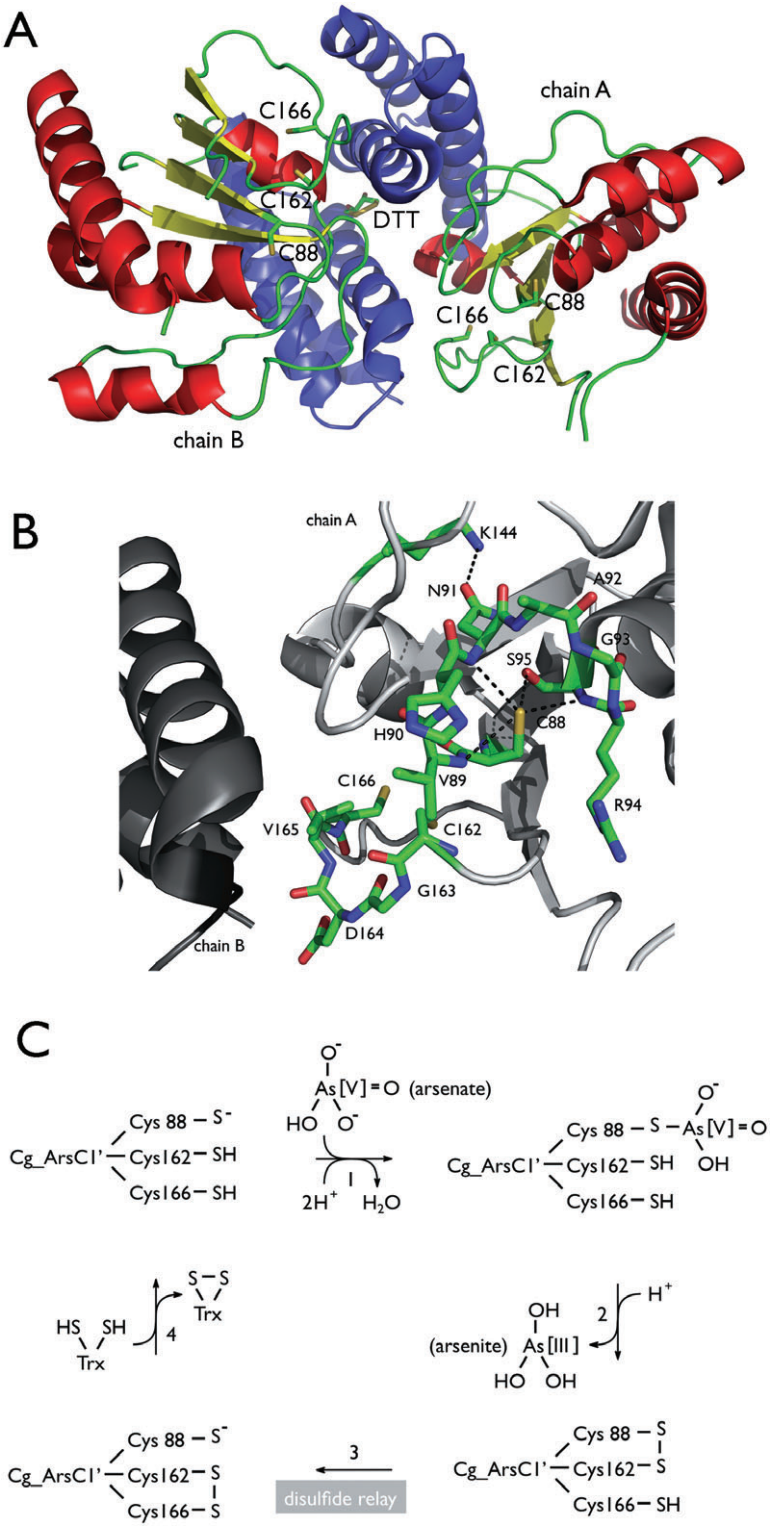

Fig. 6. Dimeric Cg_ArsC1' combines an N-terminal helical bundle with a C-terminal LMW-PTPase fold.
A. Ribbon diagram of the overall structure of Cg_ArsC1'. In both chains: the N-terminal helical bundle is in blue, the C-terminal LMW-PTPase domain is coloured by secondary structure elements. The nucleophilic cysteine (C88) and the two other essential cysteines (C162, C166) are shown. The two N-terminal helical bundles of both chains form a hydrophilic channel harbouring a molecule of DTT (present in the crystallization conditions).
B. Detailed view on the active-site P-loop and the region between C162 and C166 of Cg_ArsC1'. The hydrogen-bonding network via the asparagine 91 (N91) to the sulphur of C88 is indicated, next to its interactions with neighbouring residues. The figure was generated using MacPyMol (Delano Scientific LLC 2006).
C. Proposed catalytic reaction cycle in one monomer of Cg_ArsC1'. The reaction starts with the enzyme in the fully reduced state with anionic Cys88. (**1**) The nucleophilic attack of the thiol of Cys88 on the arsenate substrate. A hydroxyl, protonated to a water molecule, leaves. This leads to a covalent Cys88-S-$AsHO_3^-$ intermediate. Step (**2**) (the first of the disulphide relay): Cys162 attacks Cys88 with formation of a Cys88–Cys162 disulphide intermediate. The electrons from the S-As bond shuttle to arsenic and arsenite is released. Step (**3**) Cys166 attacks Cys162 forming a Cys162–Cys166 disulphide. The Cys88 thiolate is regenerated. Step (**4**) completes the reaction as reduced Cg_ArsC1' is regenerated by thioredoxin (Trx) reduction of the oxidized Cys162-Cys166 disulphide.

wavelength anomalous dispersion (Fig. 6A). Cg_ArsC1' is a homodimer and each chain of Cg_ArsC1' consists of two domains: an N-terminal bundle of three helices and a C-terminal domain with LMW-PTPase structural fold. The N-terminal domain is connected via a flexible linker to the first β-strand of the C-terminal domain, which resembles Cg_ArsC2 with a r.m.s.d. of 1.38 Å for 100 of the C-α atoms.

The active site of each chain contains three cysteines (C88, C162 and C166). The N-terminal C88 of Cg_ArsC1' is exactly in the same position as the nucleophilic cysteine (C_N) of Cg_ArsC2 in a similar P-loop structural environment (Fig. 6B). Also here, the charged $N^{\zeta}H^{+}$ of a lysine (K144) takes over the role of the potassium (observed in Sa_ArsC) as the start of a hydrogen-bonding network towards C82 via $O^{\delta 1}$ and the main chain NH of N91. Further, C88 interacts with the main chain NH of V89 and S95, and with the O^{γ} of S95 (Fig. 6B). The two other cysteines (C162 and C166) are located in a hydrophobic core separated by three residues (Gly, Asp, Val).

Based on the position of the cysteines, we can propose a similar catalytic reduction mechanism as described for Sa_ArsC (Messens *et al.*, 2002b) (Fig. 6C). The Cα of C88 is only 4.53 Å away from the Cα of C162, making this intramolecular disulphide bond likely to occur (Fig. 6C step 2). Further, the distance between the two S^{γ} of C162 and C166 is ~6.78 Å. As such, a relative small structural change might activate C166 and could reposition it to perform a nucleophilic attack on the C88–C162 disulphide forming the C162-166 disulphide (Fig. 6C step 3). From a structural point of view, a similar disulphide relay mechanism as for Sa_ArsC might be feasible to transport the oxidative equivalents to the surface of Cg_ArsC1'. New for Cg_ArsC1' is that it operates during the reduction mechanism as a homodimer. Interactions between residues of the second helix of the N-terminal helix bundle of one chain with the active-site region of the other chain might play a role during the disulphide relay mechanism.

All together, Cg_ArsC1' seems to use structural features of Sa_ArsC to reduce arsenate, but it is unique in bearing an N-terminal three helical bundle, which has never been observed in other arsenate reductases. A more detailed structure activity study will be required to solve the subtle details of this proposed reaction mechanism.

Cg_ArsC1' shows low phosphatase activity

As Cg_ArsC2 and Cg_ArsC1' are characterized by a LMW-PTPase structural fold, we decided to measure the phosphatase activity using para-nitrophenylphosphate (pNPP) as a substrate. Cg_ArsC1' showed phosphatase activity (Fig. 3E and F) with a specificity constant (k_{cat}/K_M) that is 20-fold higher than the one of pI258 Sa_ArsC (Messens *et al.*, 2002a). Nevertheless, the overall activity ($1.3\ M^{-1}\ s^{-1}$) stays far below the range (1.4×10^3 to $100 \times 10^3\ M^{-1}\ s^{-1}$) found with enzymatically characterized LMW-PTPases (Ramponi and Stefani, 1997). For Cg_ArsC1'T, Cg_ArsC1 and Cg_ArsC2 no pNPP dephosphorylation was measured (Figs 3E and S6).

How can we explain this difference? During the dephosphorylation of pNPP, a general acid needs to protonate the leaving phenolate (Wu and Zhang, 1996). In the arsenate reductase family with a LMW-PTPase fold (Fig. 1B), a plausible analogue of the general acid of the LMW-PTPase family is conserved. In Cg_ArsC1', E187, which is located on a flexible loop (density for residues 180–185 is missing), might have this role, but also E178 is a plausible general acid candidate (Fig. 1B). In Cg_ArsC2 and Cg_ArsC1, both E102 and E103 are located too far away from the nucleophilic cysteine to be functional as a general acid. For Cg_ArsC1'T, it is hard to speculate why in the absence of the N-terminal domain no phosphatase activity could be measured. No structural data are available, but for Cg_ArsC1'T the k_{cat}/K_M value for the reduction of arsenate is 10^3 times lower than for Cg_ArsC1'. The absence of the N-terminal domain might have a general impact on the structure of Cg_ArsC1'T with a loss of its de-phosphorylation activity as a consequence. In-depth kinetic studies of several mutants are needed to clarify this point.

Cg_ArsC4 has no arsenate reductase and phosphatase activity, and seems not to be involved in the survival under arsenate stress

Although Cg_ArsC4 was not expressed in *C. glutamicum* (Table 1; Fig. S1C), we decided to test whether Cg_ArsC4 is a functional arsenate reductase. We expressed Cg_ArsC4 in *E. coli*, purified it to homogeneity, and tested arsenate reductase activity linked to two electron transfer pathways present in *C. glutamicum*: the MSH/Mrx1 and the Trx/TrxR pathway (Fig. S7A and B). No electron transfer was observed.

Based on sequence-homology analysis (Fig. 1C), Cg_ArsC4 is closely related to the R773 ArsC from *E. coli* (Ec_ArsC), and therefore, one could expect an equivalent reduction mechanism for Cg_ArsC4 via a GSH/Grx electron transfer pathway (Liu *et al.*, 1995). In Actinobacteria the presence of GSH has been rarely described (Johnson *et al.*, 2009) and the low-molecular-weight thiol is MSH (Newton *et al.*, 2008). Nevertheless, we checked for arsenate reductase activity via the GSH/Grx pathway. We observed that NADPH consumption and as such electron transfer was most prominent when arsenate, GSH and Ec_Grx2 are brought together with glutathione reductase (Ec_GTR) and NADPH (Fig. S8). Adding Cg_ArsC4 to the assay gave no additional increase of NADPH consumption or reduction of arsenate. With pNPP as a substrate, no phosphatase activity could be attributed to Cg_ArsC4 (Fig. S7C). Cg_ArsC4 seems to be a non-functional arsenate reductase or at least it is not linked to one of the tested redox cycles. Furthermore, we tested the As(V) resistance with a *Cg_arsC4* gene disrupted strain and a *Cg_arsC4* gene complementation in the background

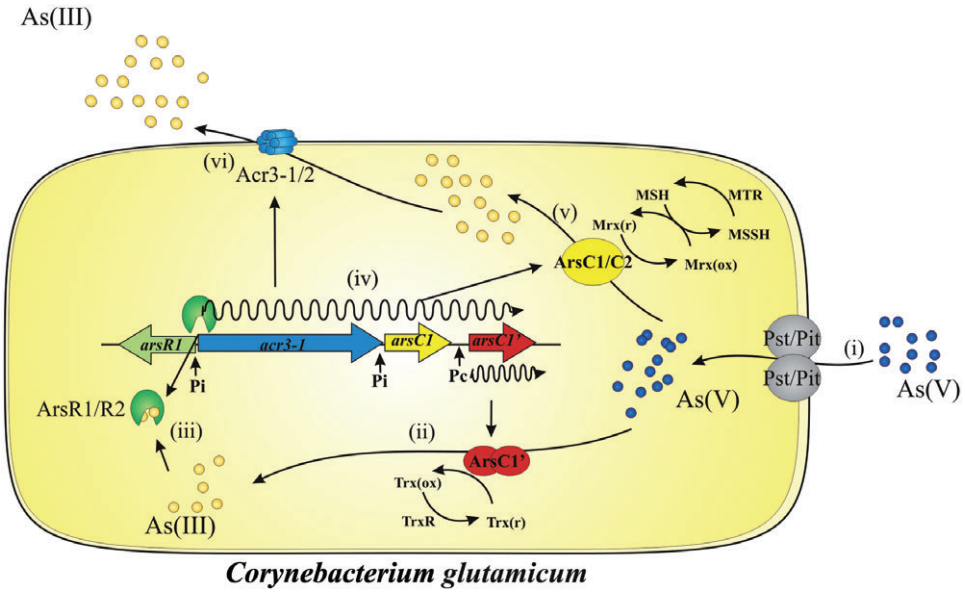

Fig. 7. The model of arsenic detoxification in *C. glutamicum*. (i) As(V) enters the cell by phosphate transports systems, (ii) the constitutive expression of the Trx-dependent ArsC1' allows immediate but controlled reduction of As(V) to As(III) (low K_M and low k_{cat}), (iii) the As(III) binds to ArsR repressors (ArsR1/R2) and structural changes makes them releasing from the *ars1* and *ars2* operons, (iv) transcription of genes from the *ars* operons, (v) the inducible arsenate reductases ArsC1/C2 are reducing As(V) to As(III) using the MSH/Mrx1-dependent reduction system, and (vi) the inducible Acr3 arsenite permeases (Acr3-1/2) on the membrane are pumping As(III) out of the cell.

strain *C. glutamicum* ArsC1–C2. No change in arsenate resistance was detected, and therefore all activity contributing to arsenic resistance seems to be absent. So, Cg_ArsC4 might have another yet to be discovered function.

Discussion

The arsenic resistance mechanism of C. glutamicum

Based on our results and on what is known from the literature, we propose the following arsenic resistance model for *C. glutamicum* (Fig. 7). Under arsenic stress in an aerobic environment, *C. glutamicum* will predominantly be exposed to arsenate, which enters the cell via the phosphate uptake system (Fig. 7, step i) (Feo *et al.*, 2007). The arsenic defence mechanism will only be induced '*in vivo*' in the presence of arsenite (Ordóñez *et al.*, 2008). In a non-arsenic environment, the ArsR repressors are bound to the *ars1* and *ars2* operator regions. To obtain gene de-repression, arsenite, produced by the basal level of Cg_ArsC1', needs to bind the ArsR repressors (Fig. 7, step iii) (Ordóñez *et al.*, 2008). In the absence of arsenite, no expression of the arsenate reductases Cg_ArsC1/C2 have been observed (Table 1). We found that Cg_ArsC1' is constitutively expressed at low levels from its own constitutive promoter (Fig. 7, step ii). If protein Cg_ArsC1' were translated from the induced polycistronic transcript, the immunodetection signal obtained for Cg_ArsC1' would be equivalent to the one obtained for Cg_ArsC1/2 and that is not the case. Therefore, it is plausible that *Cg_arsC1'* is not translated from bi- or polycistronic transcripts using the arsenite-inducible promoters, but by the newly identified constitutive promoter located upstream of Cg_*arsC1'* in the intergenic space between *Cg_arsC1* and *Cg_arsC1'* (Figs 2A and 7; see Pc upstream from *Cg_arsC1'*). Unfortunately, we were unable to observe a signal for the monocistronic mRNA of *Cg_arsC1'* on Northern blot (Ordóñez *et al.*, 2005 and this work) possibly due to very low constitutive transcription. The fact that disruption or overexpression of *Cg_arsC1'* in *C. glutamicum* showed no clear arsenate resistance phenotype is in line with our results for its poor transcription.

We showed that Cg_ArsC1' is very efficient in reducing arsenate to arsenite using electrons coming from the Trx pathway, and is characterized by a catalytic efficiency (k_{cat}/K_M) of $\sim 3 \times 10^3$ M^{-1} s^{-1} (Table 4). The expression of Cg_ArsC1' is low, but it benefits from carrying all three cysteine nucleophiles on a single evolutionary optimized polypeptide backbone chain (Fig. 6).

A single arsenate reductase (Cg_ArsC1) is already sufficient to deal with the arsenate stress, but a second copy in a second operon (Cg_ArsC2) might take over (Ordóñez *et al.*, 2009). Both arsenate reductases might even work in concert to reduce arsenate (Fig. 7, step v). Both Cg_ArsC1 and Cg_ArsC2 have a low catalytic efficiency and K_M values in the millimolar range (Table 4) (Ordóñez *et al.*,

2009). Similar kinetic parameters are observed for single cysteine arsenate reductases from other organisms (Gladysheva *et al*., 1994; Mukhopadhyay *et al*., 2000; Zhou *et al*., 2004; Duan *et al*., 2007) (Table 4). Further, the intracellular concentration of arsenic can increase to the millimolar range without affecting the viability of *C. glutamicum* (Villadangos *et al*., 2010). It is hard to speculate what happens in the cell, but local intracellular interactions might influence the catalytic efficiency. For example, we observed a dramatic change in K_M when the N-terminal interacting domain of Cg_ArsC1' was removed (see Cg_ArsC1'T in Table 4). What also needs to be taken into account is that Cg_ArsC1 and Cg_ArsC2 produce even more toxic arsenite (Lievremont *et al*., 2009), which needs to be pumped out of the cell subsequently (Fig. 7, step vi). The arsenite efflux system in *C. glutamicum* is based on two Acr3 arsenite permeases (Fu *et al*., 2009), which are working jointly in the cell although each one with a different efficiency. Using resistance to arsenite by the wild-type strain as 100%, Cg_Acr3-1 (coded in *ars1* operon) is responsible for ~80% of the arsenite efflux, while the remaining ~20% is attributed to Cg_Acr3-2 (coded in *ars2* operon) (A.F. Villadangos *et al*., unpublished).

Structure and catalytic mechanism of arsenate reductases

Cg_ArsC1' is a homodimer and each chain consists of two domains: an N-terminal helical domain, which seems to be important for dimerization and activity fine-tuning, and a C-terminal LMW-PTPase domain with the redox function.

The N-terminal domain consists of three helices. A DALI server search (Holm and Rosenstrom, 2010) showed similar helical bundles in DNA-binding and signal recognition proteins among others. As such, possible interaction with a nucleotide sequence should not be excluded at this stage. The N-terminal domain seems to be crucial for the catalytic mechanism. Its absence, like in the Cg_ArsC1'T, has a clear impact on the kinetic parameters (Table 4). Moreover, from the structure of Cg_ArsC1' (Fig. 6A) we learn that the second helix of the N-terminal helical bundle interacts with the C162–C166 region. Three residues are spacing C162 and C166 (Fig. 6B) and they are not flanking a flexible helix like in Sa_ArsC (Zegers *et al*., 2001). In the protein databank, there is another LMW-PTPase arsenate reductase from *Archaeoglobus fulgidus* (1Y1L) with the C-terminal cysteines (C_2 and C_3 in Fig. 1A) spaced by four residues, and also here, the two C-terminal cysteines do not flank a short flexible helix. This enzyme is a tetramer, but so far its catalytic function has not been described. So, it might well be that the N-terminal domain of Cg_ArsC1' plays an important structural role during the catalytic mechanism that certainly warrants further investigation.

Within the C-terminal domain, the active-site sequence motif $VLFICX_2NX_2RSQXA$ is highly conserved between ArsC1' and ArsC1'T of several organisms, and it is also characteristic for pI258 Sa_ArsC [Fig. 1A (left) and B]. Further, the structural location of C88, C162 and C166 and the reactivity features of Cg_ArsC1' coupled to Trx argue for a similar catalytic mechanism as proposed for pI258 Sa_ArsC (Fig. 6C). Next to pI258 Sa_ArsC, the *B. subtilis* arsenate reductase (Bennett *et al*., 2001) has the same fold and functions with a similar three-cysteine reduction mechanism.

An interesting feature of Sa_ArsC which has not been observed among other members of the same arsenate reductase family nor among the structurally related LMW-PTPases, is the presence of a specific potassium binding site (Lah *et al*., 2003). Previously, we have shown that the binding of K^+ is an enthalpy-driven process. K^+ binding stabilizes Sa_ArsC and increases the specific activity with a factor of 5 (Lah *et al*., 2003). Structurally, potassium is part of a hydrogen bonding network that decreases the pK_a of the nucleophilic cysteine thiol in pI258 Sa_ArsC (Roos *et al*., 2004). This potassium is important for the activity of Sa_ArsC, which we previously showed through thermodynamic cycles (Roos *et al*., 2006). In Cg_ArsC2 and in Cg_ArsC1', we see that the charged $N^{\zeta}H^+$ of the conserved Lys within this family takes over this function [Fig. 1B (the conserved Lys, respectively, K64 and K144) and in Figs 5B and 6B].

Cg_ArsC2 is the first LMW thiol-dependent arsenate reductase with a LMW-PTPase fold (Fig. 5). Arsenate reductases with a glutaredoxin fold are found in *E. coli* (PDB ID 1I9D) (Martin *et al*., 2001), in *Vibrio cholerae* (PDB ID 3F0I), *Streptococcus mutans* UA159 (PDB ID 3FZ4) and *Brucella melitensis* (PDB ID 2KOK) (Fig. 1C). Those with a rhodanese fold are *S. cerevisiae* Acr2p (Mukhopadhyay and Rosen, 2001) and *L. major* Lm_ACR2 (PDB ID 2J6P) (Mukhopadhyay *et al*., 2009). There is no relationship between Cg_ArsC2 and the tertiary structures of these arsenate reductases that function with a single nucleophilic cysteine, supporting the conclusion that Cg_ArsC2 belongs to a non-related arsenate reductase family (Fig. 1B).

Cg_ArsC1 and Cg_ArsC2 are mycothiol transferases, while Cg_ArsC1' is an arsenate reductase

Cg_ArsC1 and Cg_ArsC2 are working in concert with the MSH/Mrx1 system of the cell via an intermolecular disulphide exchange mechanism that transfers the electrons from NADPH via mycothiol disulphide reductase (Ordóñez *et al*., 2009). As Cg_Mrx1 performs the reduction of arsenate to arsenite with the release of MSH, Cg_ArsC1 and Cg_ArsC2 are functioning as an arsenate mycothiol transferase. They seems to catalyse the transfer of a molecule

of MSH to arsenate producing an arsenic-MSH adduct as substrate for Cg_Mrx1. Mechanistically, Cg_Mrx1 is performing the reduction step. Similarly, single cysteine GSH/Grx-dependent arsenate reductases could be renamed arsenate glutathione transferases. Here, Grx is performing the reduction step of arsenate to arsenite after the formation of an arsenic-GSH adduct. How mycothiol binds to the surface of the enzyme and how the nucleophilic attack occurs is still not known. The structure of Cg_ArsC2 and the biochemical data (Ordóñez *et al*., 2009) are the first glance towards the mechanism, but further in-depth structural and functional work is needed.

In contrast to the MSH/Mrx1-linked arsenate reductases Cg_ArsC1 and Cg_ArsC2, the Trx-coupled arsenate reductases like Cg_ArsC1' are terminologically referred to as real reductases (Fig. 6C). They only depend on Trx for the reduction of an intramolecular disulphide before a second catalytic cycle can be started.

Conclusion

All together, *C. glutamicum* has evolved to survive arsenate stress using many different mechanisms, which have to work in concert to pump the produced arsenite out of the cell. Remarkably, we observe two arsenate reductases families with the same structural fold, Cg_ArsC1/2 and Cg_ArsC1', which depend for the reduction of arsenate on two different thiol/disulphide relay mechanisms. Linkage to distinct redox mechanisms is not only observed for enzymes of the arsenic defence mechanism, but also for enzymes of the antioxidant defence mechanism. Some peroxidases depend on Trx (peroxiredoxins) and others on glutathione (glutathione peroxidases) (Roos and Messens, 2011). Both enzyme families are structurally related and they both remove reactive oxygen species (Toppo *et al*., 2009). It has been suggested that they may have a different role, i.e. signal transduction, oxidant scavenging, control of enzyme activity, or regulation of gene expression (Dayer *et al*., 2008; Fourquet *et al*., 2008). In *C. glutamicum*, we observe something similar. The MSH/Mrx1-linked Cg_ArsC1/2 are involved in the resistance against arsenate, while the constitutively expressed Trx-dependent Cg_ArsC1' reduces arsenate to arsenite at low levels, apparently to regulate the gene expression of Cg_ArsC1/2. It looks as if *C. glutamicum* has evolved towards the most optimal way to survive arsenic stress in an ever-changing environment.

Experimental procedures

Antibody production against Cg_ArsCs proteins and immunoblot

The native His-tagged Cg_ArsC2, Cg_ArsC1' and Cg_ArsC4 proteins obtained from the corresponding pET28a vectors were used to immunize rabbits as described (De Kerpel *et al*., 2006). Serum containing rabbit anti-Cg_ArsC2, anti-Cg_ArsC1' and anti-Cg_ArsC4 was taken after another 10 days. The resulting polyclonal antibodies were purified using protein-A Sepharose 6MB (GE Healthcare) according to the manufacturer's instructions. To study expression of Cg_ArsC proteins in the different *C. glutamicum* mutant strains, soluble proteins from *C. glutamicum* mutant strains were obtained. *C. glutamicum* cells were grown at 30°C in 100 ml of TSB media until a cell density of A_{600} = 3 was reached, and induced overnight by 1 mM As(III), if appropriate. The cells pellets were suspended in 2 ml of buffer A (vide supra) and cells disrupted by FastPrep™ FP120 as previously described. The lysate was centrifuged at 14 000 r.p.m. for 2 min and samples (10 μl) from the total supernatant (around 2 ml) were loaded on a 12% SDS-PAGE, blotted onto PVDF membranes (polyvinylidene difluoride; Millipore). Purified Cg_ArsCs proteins were used as control. Immunodetection of proteins from crude extracts was performed either (i) using specific anti-Cg_ArsCs antibodies (obtained from rabbits) at 1:1000 dilution, or (ii) with commercial antibodies directed against the His-tail (Santa Cruz technologies). Bands were visualized with anti-rabbit IgG-alkaline phosphatase conjugate (Sigma) at a 1:10 000 using commercial NBT (nitro blue tetrazolium; Sigma) and BCIP (5-bromo-1-chloro-3-indolyl phosphate; Sigma).

Arsenate reductase activity assay associated to different reduction systems

Cg_ArsC samples and Cg_Trx were unfrozen, reduced with 10 mM DTT and dialysed in a Slide-A-Lyzer Dialysis Cassette (Thermoscientific) with a molecular weight cut-off of 3500 Da against the assay buffer 20 mM Tris, pH 8.0, 150 mM NaCl (2 h with 2 buffer changes). Cg_TrxR stored as 80% ammonium sulphate pellet was resuspended in the same buffer solution prior to dialysis. For the Trx activity assay, final concentrations of 10 μM Cg_Trx, 2 μM Cg_TrxR and 250 μM NADPH were used, taking into account the subsequent addition of arsenate and the respective tested enzymes Cg_ArsC1', Cg_ArsC1'T and Cg_ArsC4, each at 500 nM. For the GSH/Grx2 activity assay, Ec_Grx2 was expressed and purified as described (Shi *et al*., 1999), with a final yield of 39 mg per litre of culture. In the assay buffer solution (50 mM MES, pH 6.5), final concentrations of 500 μM NADPH, 3 μM glutathione reductase (GTR, Sigma), 5 mM glutathione (GSH, Sigma), 20 μM Ec_Grx2, 5 μM Cg_ArsC4 and 100 mM As(V) were used. For the MSH/Mrx activity assay, Cg_Mrx1, Cg_MTR and MSH were purified as described (Ordóñez *et al*., 2009). The final assay mixture was prepared by diluting all components in the assay buffer solution (10 μM Cg_Mrx1, 3 μM Cg_MTR, 0.47 mM MSH and 250 μM NADPH final concentration), except for Cg_ArsC1', Cg_ArsC1'T or Cg_ArsC4 and its substrate arsenate, taking into account the subsequent addition of varying concentrations of arsenate and the respective enzymes at 200 nM. As control, Cg_ArsC2 was used (Ordóñez *et al*., 2009).

Kinetics by evaluating the NADPH consumption

The component mixture and different dilution series of substrate were mixed and incubated for 20 min at 37°C in a

96-well plate (PolySorb, Nunc, Denmark) (180 µl well^{-1}) in a SPECTRA- max 340PC (Molecular Devices, Sunnyvale, CA). The assay was started by the addition of enzyme in the case of the MSH/Mrx pathway assay or by the addition of arsenate in the case of the Trx pathway assay (20 µl well^{-1}) to obtain a final volume of 200 µl well^{-1}. As a background control for the assay, buffer solution was added. The arsenate reduction coupled to NADPH oxidation ($\Delta\varepsilon_{340}$ = 6220 M^{-1} cm^{-1}) was measured by following the decrease in absorption at 340 nm. The path length was measured after each run for each well with the PathCheck Sensor of the system and was used for k_{cat} calculations. Initial rates were calculated with SPECTRAmaxPro (Molecular Devices). Kinetic plots were made with Prism version 5.0 using the Michaelis–Menten expression to calculate V_{max} and k_{cat} values.

Phosphatase activity assay

The pNPP phosphatase activity assay was performed as described (Zegers *et al*., 2001). Briefly, the phosphatase activity was measured with 5 µM Cg_ArsC1'/Cg_ArsC1'T/Cg_ArsC4/Cg_ArsC1/Cg_ArsC2 in 100 mM Na citrate, pH 6.7, 150 mM KCl, 0.1 mM EDTA. ArsCs were incubated without substrate at 37°C in a 96-well plate (180 µl per well) in a SPECTRAmax340PC for 5 min. The assay was started by the addition of dilution series of pNPP (20 µl per well). The dephosphorylation of pNPP ($\Delta\varepsilon_{405}$ = 18 000 M^{-1} cm^{-1}) was measured by following the increase in absorption at 405 nm. Each substrate dilution point was corrected for non-enzymatic pNPP dephosphorylation and the path length of the well. Initial rates were calculated with SPECTRAmaxPro. Kinetic plots were made with the MM expression to calculate the K_M, V_{max} and k_{cat}.

Quantification of the arsenic content in C. glutamicum

Corynebacterium glutamicum strains were pre-cultured overnight in TSB medium under continuous stirring. Pre-cultures (0.6 ml) were used to inoculate 60 ml (1%) of MMCLP minimal medium (described in media) and cultured until a cell density of A_{600} = 2. Cells were harvested, washed twice in 30 ml of TAB solution (75 mM HEPES, pH 7.3, 150 mM KCl and 1 mM $MgCl_2$) (Villadangos *et al*., 2010), and the pellet was resuspended in a final volume of 2 ml of TAB solution, which allowed storage of the cells in a non-growing state ('resting cells'). The 'resting cells' (100 µl) were added to 900 µl of TAB solution at 30°C containing 100 µM of As(V) or different arsenate concentration when indicated, and at varying retention times (1–180 min), 100 µl of the cells-arsenic solution was filtered (nitrocellulose 0.45 µm filters; Millipore). The retained cells were washed twice with 5 ml of TAB solution to remove residual arsenate on a filter manifold (Hoefer FH 225V) connected to a vacuum pump. Filters and retained cells were then dissolved in 70% nitric acid (HNO_3) at 65°C and diluted with HPLC grade water to bring each sample to a final concentration of 1% HNO_3. The amount of arsenic retained by the 'resting cells' biomass was directly determined by inductively coupled plasma-mass spectrometry (ICP-MS; ELAN 9000 PerkinElmer). As(V) standards were used to calibrate the instrument, and the experimental data are the mean of three replicates.

Arsenite and arsenate analysis with atomic fluorescence spectroscopy

All components (or an experimentally designed selection) of the *Arsenate reductase activity assay* (vide supra) were mixed in 10 mM Bis-tris/HCl, pH 6.5, or 50 mM Tris pH 7.7 (Cg_ArsC1' and Cg_ArsC1'T), using the respective concentrations of the kinetic assays together with 75 mM As(V) for Cg_ArsC1'/Cg_ArsC1'T. For the reaction with Mrx1, MSH, MTR and NADPH, we used the described conditions (Ordóñez *et al*., 2009). After 2 h of incubation at 37°C, the reaction was stopped by removing the proteins on a solid-phase extraction cartridge (Waters Oasis HLB). For Cg_ArsC4, the following reaction mixture [NADPH (500 µM), Ec_GTR (3 µM), GSH (5 mM), Ec_Grx2 (20 µM), Cg_ArsC4 (5 µM), As(V) (100 mM)] was used, and the reaction was stopped after 20 min. The excess of arsenate was removed on Dowex 21 K/XLT anion exchange resin (Supelco) pre-treated with NaCl in Bis-tris/HCl, pH 6.5, and thoroughly washed with water. The flow-through fraction was 0.2 µm filtered, argon-flushed, and injected on a Hamilton PRP-X100 anion exchange column (250 × 4.1 mm) operated in 20 mM KH_2PO_4/K_2HPO_4, pH 6.0, at 1 ml min^{-1}. The high-pressure liquid chromatography effluent was mixed with 1.5 M HCl and 2.5% $NaBH_4$, 2% NaOH at 1 ml min^{-1} to form gaseous arsine (AsH_3). The arsines were analysed and quantified using an atomic fluorescence spectrometer (Excalibur, PS Analytical, Orpington, UK) calibrated with a standard of arsenite and arsenate.

Protein crystallization

Purified Cg_ArsC2 (Ordóñez *et al*., 2009) (13.7 mg ml^{-1}) was mixed with an equal volume (1 µl) of reservoir solution. Cg_ArsC2 was crystallized at 293 K with the hanging drop vapour diffusion method in 20% PEG 10000, 0.1 M HEPES pH 7.5 (Hampton Research, CA, USA) in the bottom solution (0.5 ml) after ~ 12 months of incubation. Purified Cg_ArsC1' (15 mg ml^{-1}) was crystallized by using the sitting-drop vapour diffusion method at 293 K using a nanodrop dispensing robot (Phoenix Art Robbins instruments) in 96 three-well crystallization plates. Cg_ArsC1' crystallized in 0.1 M Tris/HCl pH 8.0, 32% PEG 4000 (Hampton Research, CA, USA), and in 50 mM Tris/HCl pH 8.0, 0.1 M $NaClO_4$, 30% PEG 4000 (Messens *et al*., 2004) after 2- to 3-day incubation.

Escherichia coli BL21(DE3) transformed with pETarsC1' was grown in minimal medium (Zegers *et al*., 2001) in the presence of 50 µg ml^{-1} kanamycin. At a cell density of A_{600} of ~ 0.7, 13.2 mg l^{-1} culture of each amino acid (except methionine) and selenomethionine were added, and the expression was induced by the addition of 1 mM IPTG. Cells were harvested after an overnight growth at 23°C. SeMet Cg_ArsC1' was purified as described. Dimeric SeMet Cg_ArsC1' was concentrated to 6 mg ml^{-1} in 20 mM Tris/HCl, pH 8.0, 150 mM NaCl and 1 mM DTT and crystallized by hanging drop in 26% PEG 4000, 0.1 M Tris/HCl pH 8.0, 5 mM DTT. Crystals grew in 3 days at 293 K.

Data collection and structure determinations

Data of Cg_ArsC2 and Cg_ArsC1' were collected at 100 K at beamline ID23-1 of the ESRF synchrotron in Grenoble, France. Diffraction images were processed using the programs DENZO, XDisplayF and SCALEPACK from the HKL Package (Otwinowski and Minor, 1997) and the CCP4 program TRUNCATE (Collaborative Computational Project, 1994). The structure of Cg_ArsC2 was determined by molecular replacement using *B. subtilis* ArsC (PDB code: 1JE3) (Bennett *et al*., 2001). The C-terminal part of the structure of Cg_ArsC1' was determined by molecular replacement using Sa_ArsC (PDB code: 2CD7) (Roos *et al*., 2006). Refinement cycles using the maximum likelihood target function of phenix.refine (Afonine *et al*., 2005) and REFMAC (Murshudov *et al*., 1997) were alternated with manual building using Coot (Emsley and Cowtan, 2004).

The structure of selenomethionine-labelled Cg_ArsC1' was solved using single wavelength anomalous dispersion (SAD, Se-peak). Diffraction data were collected at the PROXIMA1 beamline of the SOLEIL Synchrotron, Paris, France. Data were processed using XDS (Kabsch, 2010). Four selenium sites were found using SHELXD (Sheldrick and Schneider, 1997). The obtained phases were improved by density modification using Parrot and the initial model built using Buccaneer found in the CCP4 suite (Collaborative Computational Project, 1994). The model from Buccaneer was further built using ARP/WARP (Langer *et al*., 2008). The model from ARP/WARP was then used for iterative manual building and refinement with COOT (Emsley and Cowtan, 2004) and REFMAC5 (Murshudov *et al*., 1997) respectively. The statistics of the refinement are shown in Table S4.

Online supplemental experimental procedures

- Strains, plasmids, media and reagents
- Primers used for PCR amplification and sequencing (Table S3)
- DNA and RNA manipulations
- Computer analysis
- Promoter strength evaluation
- *Cg_arsC1'* and *Cg_arsC4* gene disruption in *C. glutamicum*
- His-codon addition to the chromosomal genes *Cg_arsC1'* and *Cg_arsC4* and purification of his-tagged proteins from *C. glutamicum*
- Assays for complementation of the arsenate reductase activity by subgene *Cg_arsC1'T* and the cluster *Cg_arsC1–Cg_arsC1'*
- Arsenic resistance analysis
- Cloning, expression and purification of *Cg_arsC1'*, *Cg_arsC1'T* and *Cg_arsC4* in *E. coli*
- Analytical reversed phase chromatography (RPC)
- Mass spectrometry and concentration determination
- Selwyn's test of enzyme inactivation
- Determination of the pKa of the nucleophilic cysteine of Cg_ArsC1 and Cg_ArsC2

Acknowledgements

We would like to thank Wael Gad and Lea Brys for immunizations, Koen Verschueren for data collection, Guy Vanden-Bussche for mass spec analysis and Lieven Buts for docking experiments with AutoDock. V.T.D. is funded by ISRIB and WELBIO. A.F.V. is beneficiary of a fellowship from Junta de Castilla y León. L.M.M. and J.A.G. are benefits of the Spanish grants: Junta de Castilla y León (LE028A10-2), and Ministerio de Ciencia e Innovación (BIO2008-00519). J.M. is a group leader of the VIB. Part of this work was funded by a HOA grant of the VUB. The authors acknowledge use of synchrotron beamtime at the ESRF (Grenoble France) and SOLEIL (Paris France).

References

Achour, A.R., Bauda, P., and Billard, P. (2007) Diversity of arsenite transporter genes from arsenic-resistant soil bacteria. *Res Microbiol* **158:** 128–137.

Afonine, P.V., Grosse-Kunstleve, R.W., and Adams, P.D. (2005) A robust bulk-solvent correction and anisotropic scaling procedure. *Acta Crystallogr D Biol Crystallogr* **61:** 850–855.

Bennett, M.S., Guan, Z., Laurberg, M., and Su, X.D. (2001) *Bacillus subtilis* arsenate reductase is structurally and functionally similar to low molecular weight protein tyrosine phosphatases. *Proc Natl Acad Sci USA* **98:** 13577–13582.

delCardayre, S.B., Stock, K.P., Newton, G.L., Fahey, R.C., and Davies, J.E. (1998) Coenzyme A disulfide reductase, the primary low molecular weight disulfide reductase from *Staphylococcus aureus*. Purification and characterization of the native enzyme. *J Biol Chem* **273:** 5744–5751.

Chenna, R., Sugawara, H., Koike, T., Lopez, R., Gibson, T.J., Higgins, D.G., and Thompson, J.D. (2003) Multiple sequence alignment with the Clustal series of programs. *Nucleic Acids Res* **31:** 3497–3500.

Collaborative Computational Project (1994) The CCP4 suite: programs for protein crystallography. *Acta Crystallogr D Biol Crystallogr* **50:** 760–763.

Collet, J.F., and Messens, J. (2010) Structure, function, and mechanism of thioredoxin proteins. *Antioxid Redox Signal* **13:** 1205–1216.

Dayer, R., Fischer, B.B., Eggen, R.I., and Lemaire, S.D. (2008) The peroxiredoxin and glutathione peroxidase families in *Chlamydomonas reinhardtii*. *Genetics* **179:** 41–57.

De Kerpel, M., Van Molle, I., Brys, L., Wyns, L., De Greve, H., and Bouckaert, J. (2006) N-terminal truncation enables crystallization of the receptor-binding domain of the FedF bacterial adhesin. *Acta Crystallogr Sect F Struct Biol Cryst Commun* **62:** 1278–1282.

Duan, G.L., Zhou, Y., Tong, Y.P., Mukhopadhyay, R., Rosen, B.P., and Zhu, Y.G. (2007) A CDC25 homologue from rice functions as an arsenate reductase. *New Phytol* **174:** 311–321.

Emsley, P., and Cowtan, K. (2004) Coot: model-building tools for molecular graphics. *Acta Crystallogr D Biol Crystallogr* **60:** 2126–2132.

Fahey, R.C. (2001) Novel thiols of prokaryotes. *Annu Rev Microbiol* **55:** 333–356.

Feo, J.C., Ordóñez, E., Letek, M., Castro, M.A., Munoz, M.I., Gil, J.A., *et al*. (2007) Retention of inorganic arsenic by coryneform mutant strains. *Water Res* **41:** 531–542.

Fourquet, S., Huang, M.E., D'Autreaux, B., and Toledano, M.B. (2008) The dual functions of thiol-based peroxidases

in H2O2 scavenging and signaling. *Antioxid Redox Signal* **10:** 1565–1576.
Fu, H.L., Meng, Y., Ordonez, E., Villadangos, A.F., Bhattacharjee, H., Gil, J.A., *et al.* (2009) Properties of arsenite efflux permeases (Acr3) from *Alkaliphilus metalliredigens* and *Corynebacterium glutamicum*. *J Biol Chem* **284:** 19887–19895.
Gladysheva, T.B., Oden, K.L., and Rosen, B.P. (1994) Properties of the arsenate reductase of plasmid R773. *Biochemistry* **33:** 7288–7293.
Guo, X., Li, Y., Peng, K., Hu, Y., Li, C., Xia, B., and Jin, C. (2005) Solution structures and backbone dynamics of arsenate reductase from *Bacillus subtilis*: reversible conformational switch associated with arsenate reduction. *J Biol Chem* **280:** 39601–39608.
Helmann, J.D. (2011) Bacillithiol, a new player in bacterial redox homeostasis. *Antioxid Redox Signal* **15:** 123–133.
Holm, L., and Rosenstrom, P. (2010) Dali server: conservation mapping in 3D. *Nucleic Acids Res* **38:** W545–W549.
Johnson, T., Newton, G.L., Fahey, R.C., and Rawat, M. (2009) Unusual production of glutathione in Actinobacteria. *Arch Microbiol* **191:** 89–93.
Jothivasan, V.K., and Hamilton, C.J. (2008) Mycothiol: synthesis, biosynthesis and biological functions of the major low molecular weight thiol in actinomycetes. *Nat Prod Rep* **25:** 1091–1117.
Kabsch, W. (2010) Xds. *Acta Crystallogr D Biol Crystallogr* **66:** 125–132.
Kulp, D., Haussler, D., Reese, M.G., and Eeckman, F.H. (1996) A generalized hidden Markov model for the recognition of human genes in DNA. *Proc Int Conf Intell Syst Mol Biol* **4:** 134–142.
Lah, N., Lah, J., Zegers, I., Wyns, L., and Messens, J. (2003) Specific potassium binding stabilizes pI258 arsenate reductase from *Staphylococcus aureus*. *J Biol Chem* **278:** 24673–24679.
Langer, G., Cohen, S.X., Lamzin, V.S., and Perrakis, A. (2008) Automated macromolecular model building for X-ray crystallography using ARP/wARP version 7. *Nat Protoc* **3:** 1171–1179.
Li, R., Haile, J.D., and Kennelly, P.J. (2003) An arsenate reductase from *Synechocystis* sp. strain PCC 6803 exhibits a novel combination of catalytic characteristics. *J Bacteriol* **185:** 6780–6789.
Lievremont, D., Bertin, P.N., and Lett, M.C. (2009) Arsenic in contaminated waters: biogeochemical cycle, microbial metabolism and biotreatment processes. *Biochimie* **91:** 1229–1237.
Liu, J., Gladysheva, T.B., Lee, L., and Rosen, B.P. (1995) Identification of an essential cysteinyl residue in the ArsC arsenate reductase of plasmid R773. *Biochemistry* **34:** 13472–13476.
Martin, P., DeMel, S., Shi, J., Gladysheva, T., Gatti, D.L., Rosen, B.P., and Edwards, B.F. (2001) Insights into the structure, solvation, and mechanism of ArsC arsenate reductase, a novel arsenic detoxification enzyme. *Structure* **9:** 1071–1081.
Masip, L., Veeravalli, K., and Georgiou, G. (2006) The many faces of glutathione in bacteria. *Antioxid Redox Signal* **8:** 753–762.
Messens, J., and Silver, S. (2006) Arsenate reduction: thiol cascade chemistry with convergent evolution. *J Mol Biol* **362:** 1–17.
Messens, J., Martins, J.C., Brosens, E., Van Belle, K., Jacobs, D.M., Willem, R., and Wyns, L. (2002a) Kinetics and active site dynamics of *Staphylococcus aureus* arsenate reductase. *J Biol Inorg Chem* **7:** 146–156.
Messens, J., Martins, J.C., Van Belle, K., Brosens, E., Desmyter, A., De Gieter, M., *et al.* (2002b) All intermediates of the arsenate reductase mechanism, including an intramolecular dynamic disulfide cascade. *Proc Natl Acad Sci USA* **99:** 8506–8511.
Messens, J., Van Molle, I., Vanhaesebrouck, P., Van Belle, K., Wahni, K., Martins, J.C., *et al.* (2004) The structure of a triple mutant of pI258 arsenate reductase from *Staphylococcus aureus* and its 5-thio-2-nitrobenzoic acid adduct. *Acta Crystallogr D Biol Crystallogr* **60:** 1180–1184.
Mukhopadhyay, R., and Rosen, B.P. (1998) *Saccharomyces cerevisiae ACR2* gene encodes an arsenate reductase. *FEMS Microbiol Lett* **168:** 127–136.
Mukhopadhyay, R., and Rosen, B.P. (2001) The phosphatase C(X)5R motif is required for catalytic activity of the *Saccharomyces cerevisiae* Acr2p arsenate reductase. *J Biol Chem* **276:** 34738–34742.
Mukhopadhyay, R., and Rosen, B.P. (2002) Arsenate reductases in prokaryotes and eukaryotes. *Environ Health Perspect* **110:** 745–748.
Mukhopadhyay, R., Shi, J., and Rosen, B.P. (2000) Purification and characterization of ACR2p, the *Saccharomyces cerevisiae* arsenate reductase. *J Biol Chem* **275:** 21149–21157.
Mukhopadhyay, R., Bisacchi, D., Zhou, Y., Armirotti, A., and Bordo, D. (2009) Structural characterization of the As/Sb reductase LmACR2 from *Leishmania major*. *J Mol Biol* **386:** 1229–1239.
Murshudov, G.N., Vagin, A.A., and Dodson, E.J. (1997) Refinement of macromolecular structures by the maximum-likelihood method. *Acta Crystallogr D Biol Crystallogr* **53:** 240–255.
Newton, G.L., Buchmeier, N., and Fahey, R.C. (2008) Biosynthesis and functions of mycothiol, the unique protective thiol of Actinobacteria. *Microbiol Mol Biol Rev* **72:** 471–494.
Ordóñez, E., Letek, M., Valbuena, N., Gil, J.A., and Mateos, L.M. (2005) Analysis of genes involved in arsenic resistance in *Corynebacterium glutamicum* ATCC 13032. *Appl Environ Microbiol* **71:** 6206–6215.
Ordóñez, E., Thiyagarajan, S., Cook, J.D., Stemmler, T.L., Gil, J.A., Mateos, L.M., and Rosen, B.P. (2008) Evolution of metal(loid) binding sites in transcriptional regulators. *J Biol Chem* **283:** 25706–25714.
Ordóñez, E., Van Belle, K., Roos, G., De Galan, S., Letek, M., Gil, J.A., *et al.* (2009) Arsenate reductase, mycothiol, and mycoredoxin concert thiol/disulfide exchange. *J Biol Chem* **284:** 15107–15116.
Otwinowski, Z., and Minor, W. (1997) Processing of X-ray diffraction data collected in oscillation mode. *Methods Enzymol* **276:** 307–326.
Ramponi, G., and Stefani, M. (1997) Structure and function of the low Mr phosphotyrosine protein phosphatases. *Biochim Biophys Acta* **1341:** 137–156.
Rawat, M., and Av-Gay, Y. (2007) Mycothiol-dependent pro-

teins in actinomycetes. *FEMS Microbiol Rev* **31:** 278–292.
Roos, G., and Messens, J. (2011) Protein sulfenic acid formation: from cellular damage to redox regulation. *Free Radic Biol Med* **51:** 314–326.
Roos, G., Messens, J., Loverix, S., Wyns, L., and Geerlings, P. (2004) A computational and conceptual DFT study on the Michaelis complex of pI258 arsenate reductase. Structural aspects and activation of the electrophile and nucleophile. *J Phys Chem B* **108:** 17216–17225.
Roos, G., Buts, L., Van Belle, K., Brosens, E., Geerlings, P., Loris, R., *et al*. (2006) Interplay between ion binding and catalysis in the thioredoxin-coupled arsenate reductase family. *J Mol Biol* **360:** 826–838.
Selwyn, M.J. (1965) A simple test for inactivation of an enzyme during assay. *Biochim Biophys Acta* **105:** 193–195.
Sheldrick, G., and Schneider, T. (1997) SHELXL: high-resolution refinement. *Methods Enzymol* **277:** 319–343.
Shi, J., Vlamis-Gardikas, A., Aslund, F., Holmgren, A., and Rosen, B.P. (1999) Reactivity of glutaredoxins 1, 2, and 3 from *Escherichia coli* shows that glutaredoxin 2 is the primary hydrogen donor to ArsC-catalyzed arsenate reduction. *J Biol Chem* **274:** 36039–36042.
Toppo, S., Flohé, L., Ursini, F., Vanin, S., and Maiorino, M. (2009) Catalytic mechanisms and specificities of glutathione peroxidases: variations of a basic scheme. *Biochim Biophys Acta* **1790:** 1486–1500.
Villadangos, A.F., Ordonez, E., Munoz, M.I., Pastrana, I.M., Fiuza, M., Gil, J.A., *et al*. (2010) Retention of arsenate using genetically modified coryneform bacteria and determination of arsenic in solid samples by ICP-MS. *Talanta* **80:** 1421–1427.
Wu, L., and Zhang, Z.Y. (1996) Probing the function of Asp128 in the lower molecular weight protein-tyrosine phosphatase-catalyzed reaction. A pre-steady-state and steady-state kinetic investigation. *Biochemistry* **35:** 5426–5434.
Yu, C., Xia, B., and Jin, C. (2011) 1H, 13C and 15N resonance assignments of the arsenate reductase from *Synechocystis* sp. strain PCC 6803. *Biomol NMR Assign* **5:** 85–87.
Zegers, I., Martins, J.C., Willem, R., Wyns, L., and Messens, J. (2001) Arsenate reductase from *S. aureus* plasmid pI258 is a phosphatase drafted for redox duty. *Nat Struct Biol* **8:** 843–847.
Zhou, Y., Messier, N., Ouellette, M., Rosen, B.P., and Mukhopadhyay, R. (2004) *Leishmania major* LmACR2 is a pentavalent antimony reductase that confers sensitivity to the drug pentostam. *J Biol Chem* **279:** 37445–37451.

Supporting information

Additional supporting information may be found in the online version of this article.

Please note: Wiley-Blackwell are not responsible for the content or functionality of any supporting materials supplied by the authors. Any queries (other than missing material) should be directed to the corresponding author for the article.